# Single-Walled Carbon Nanotube-Induced Orthogonal Growth of Polyethylene Single Crystals at a Curved Liquid/Liquid Interface

Wenda Wang and Christopher Y. Li*

Department of Materials Science and Engineering, Drexel University, Philadelphia, Pennsylvania 19104, United States

S *Supporting Information*

ABSTRACT: We report herein single-walled carbon nanotube-induced polyethylene crystallization at the curved liquid/liquid interface. A Pickering emulsion system comprised of polyethylene (PE)/single-walled carbon nanotubes (SWCNTs)/1,2-dichlorobenzene (DCB)/water is formed using probe sonication at an elevated temperature. SWCNTs are used as the Pickering agents, and they are bent into nanosized rings by the curved DCB/water interface. Upon cooling, PE crystallizes onto SWCNTs, forming kebab single crystals, and the PE lamellae are orthogonal to the DCB/water interface. The unique structure resembles nanohybrid shish kebab (NHSK) rings.
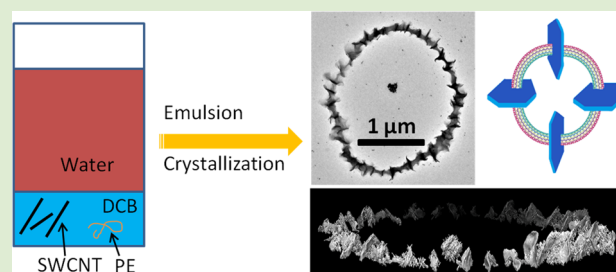
$\mathbf{P}$olymer crystallization confined at the liquid/liquid interface (L/L) has attracted increasing attention during the past decade. One such example can be found in crystalline polymer blends, where L/L phase separation (e.g., spinodal decomposition) couples with crystallization.[1] For polymer solution crystallization, a different scenario arises, and polymer single crystals may form at the L/L interface.[2] Lotz et al. reported that, in polyethylene (PE) solution crystallization, upon cooling the solution from high temperature, L/L phase separation can occur prior to PE crystallization.[2a] In such a case, PE crystalline microspheres are formed with a distinct smooth or rough surface due to homogeneous or heterogeneous nucleation, respectively. To decouple these two nucleation processes and study the interface/nucleation effect on crystallization, it is desirable to precisely locate nucleation agents at the L/L interface. One possible strategy to achieve such a goal is using Pickering emulsion.

In a water/oil/colloidal particle (W/O/P) system, particles tend to segregate into a water/oil (W/O) interface to lower the overall free energy of the system, a phenomenon known as Pickering emulsion.[3] The stability of the emulsion depends on particle diameter and the interfacial energy between P/O, P/W, and W/O.[4] Numerous micro- and nanoparticles have been studied in Pickering emulsion systems.[5] In addition to spherical nanoparticles, anisotropic nanorods[6] and carbon nanotubes (CNTs)[7] have also been assembled at the L/L interface. We have recently showed that single-walled carbon nanotubes (SWCNTs) can be used as Pickering agents to create miniemulsion, where the SWCNTs are bent into nanorings with a diameter ranging from 100 nm to ~micrometers.[8] Because SWCNTs have been used to nucleate crystallization of numerous polymers,[9] the precise location of the SWCNT at the W/O interface provides a unique opportunity to study heterogeneous nucleation at the L/L interface. Herein we report PE solution crystallization in a Pickering emulsion

system where SWCNTs are used as the Pickering agents. SWCNT-induced PE single-crystal growth at the W/O interface in this system leads to a unique hybrid structure with the SWCNT bundles forming a nanosized ring, and polymer crystals align orthogonal to the W/O interface. The overall structure mimics a nanospike necklace. Of interest is that, disregarding the significant different surface tension of water and oil, the polymer single crystals show similar growth rates in these two phases, orthogonal to the SWCNT axis. A detailed growth mechanism will be discussed.

Scheme 1a shows our PE solution crystallization process in a SWCNT-stabilized Pickering emulsion. In brief, 0.01 wt % SWCNTs are dispersed in 1,2-dichlorobenzene (DCB) using probe sonication at room temperature. The dispersion is brought to 98 °C and equilibrated for 10 min. A PE/DCB solution with a concentration of 0.01 wt % is prepared at 120 °C and cooled to 98 °C. A 0.1 mL SWNCT dispersion is then mixed with 0.1 mL of PE/DCB solution and 8 mL of water. The system is subject to 10 min probe sonication to yield an emulsion, which then is quenched to room temperature for crystallization for approximately 15 min. PE is chosen as the model polymer because of its well-known crystalline structure, morphology, and crystallization behavior in DCB. In addition, SWCNTs are known to be able to induce PE crystallization, and a unique nanohybrid shish kebab (NHSK) structure, where SWCNTs act as the shish and PE single crystals as the kebabs, has been observed in solution, thin film, and bulk PE/SWCNT systems.[10] Figure 1a shows a typical transmission electron microscopy (TEM) bright field image of NHSK nucleated by

Scheme 1. (a) Fabrication Process of NHSK Rings Using Controlled Nucleation/Crystallization at the L/L Interface and (b) Formation Process of SWCNT-Stabilized Droplets and the Orthogonal Crystallization Process at the L/L Interface
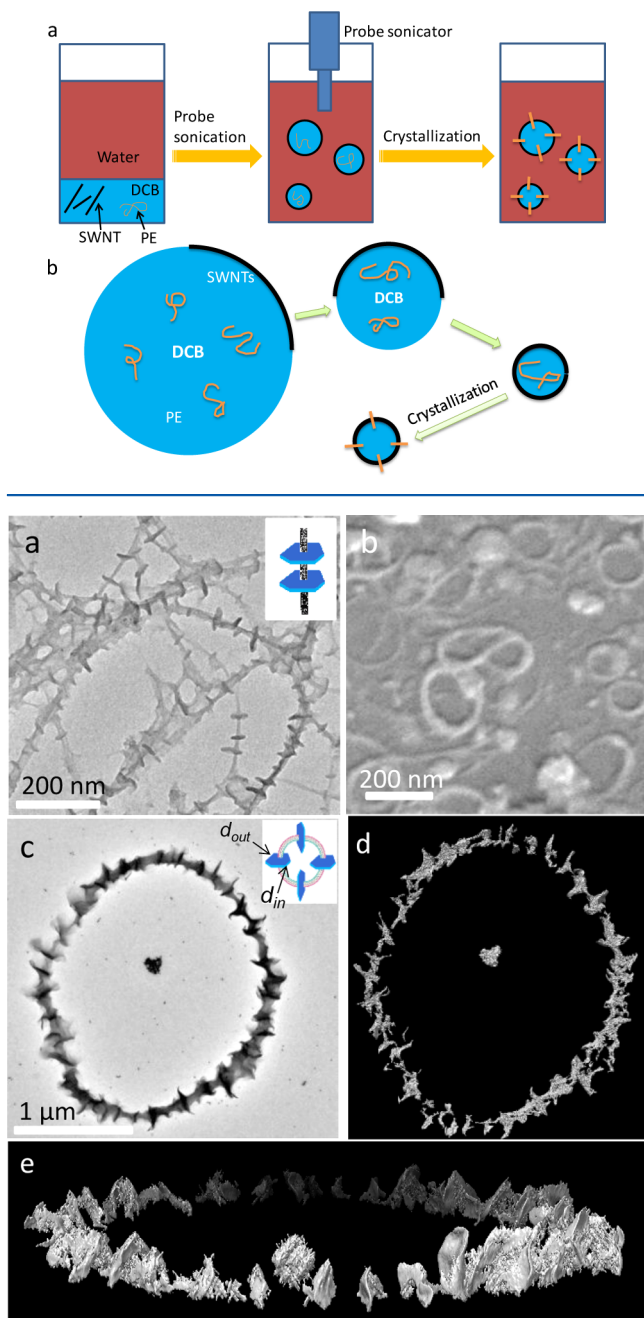

Figure 1. (a) TEM image of straight NHSK. The inset shows the schematics of the NHSK. (b) SEM micrograph of bare SWCNT rings. (c) Bright-field TEM image of an NHSK ring formed using a 1:1 PE/ SWCNT ratio. The inset shows the schematics of the NHSK ring. (d) and (e) show the top and tilted view of the reconstructed image of (c) using TEM tomography.

SWCNTs in solution. The inset in Figure 1a is a schematic representation of an NHSK.

Figure 1b shows typical SWCNT nanorings formed at the curved water/DCB interface upon Pickering emulsion.[8] A bundle of SWCNTs is bent to follow the curved L/L interface

and eventually forms an enclosed nanosized ring (Scheme 1b). A detailed SWCNT ring formation process has been reported previously.[8] Using these SWCNT nanorings as the nucleation agent and following the above-discussed procedure, PE single crystals can be controlled to grow at the L/L interface. Figure 1c displays a bright-field TEM micrograph of the resultant structure grown from the Pickering emulsion system with a 1:1 PE/SWCNT weight ratio. A ring-shaped nanohybrid shish-kebab structure (NHSK nanoring) is formed, and the entire hybrid also mimics a nanospike necklace. PE chains crystallize along the surface of the SWCNTs, forming crystalline lamellae wrapping around the nanotube backbone. Edge-on PE crystals are strung together by SWCNTs. In Figure 1c, the overall diameter of the hybrid ring is ca. 2 μm; there are ~50 edge-on PE lamellar single crystals grown on the ring; and each lamella is ca. 200 nm wide. To better characterize the 3-dimensional (3D) structure of the hybrid ring, TEM tomography was employed.[11] The small black dots in Figure 1c−e are gold nanoparticles (AuNPs), which were used as fiducial markers to align the tilt series images during tomography reconstruction. Images were collected from −60° to +60° with an interval of 1.5°. Figure 1d and 1e are the top and tilted view of the reconstructed images of the hybrid ring in Figure 1c. A 3D rotation movie of the reconstructed hybrid ring can be found in the Supporting Information. The formation of this NHSK nanoring suggests that SWCNTs are bent into nanorings first during the miniemulsion process. After being quenched to room temperature, PE starts to crystallize (Scheme 1b). Figure 1d,e and the video in the Supporting Information show that the PE lamellae are orthogonal to the SWNT ring plane, indicating that SWCNTs are the nucleation agents for PE crystallization.

In a typical PE NHSK (Figure 1a), the PE crystal grows orthogonal to the CNT axis, and the formation process is governed by the size-dependent soft-epitaxial growth mechanism as previously reported.[10d,12] To elucidate the chain orientation relative to the SWCNT, selected area electron diffraction (SAED) was employed. Figure 2 shows the TEM
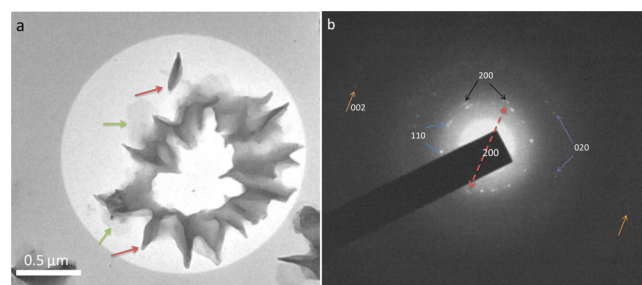

Figure 2. TEM micrograph of a NHSK ring (a) and its corresponding electron diffraction pattern (b).

image of an individual NHSK nanoring and its corresponding SAED pattern with the correct orientation. On the basis of the previous argument, each kebab crystal should contribute one pair of (002) diffractions with [002] perpendicular to the lamellar surface. However, in Figure 2b, only one pair of (002) is observed, which can be associated with two kebab lamellae in Figure 2a (indicated by red arrows). Besides (002), multiple pairs of (200), (110), and (020) diffraction spots can be observed in the pattern. Indicated by a double-headed arrow in Figure 2b is the (200) pair that is from the two highlighted (red arrow) kebabs in Figure 2a. Lack of (002) diffraction from most kebabs and the observation of multiple sets of (200), (110),

and (020) can be attributed to deformation of PE lamellae upon sample preparation. Because PE lamellae are thin and do not have a uniform size, upon deposition, they tend to deform and are therefore tilted from the film normal. The corresponding (002) diffractions are then tilted away from the registration plane and are absent from the shown diffraction pattern. The collapsed lamellae (green arrows) also produce (*hk*0) diffractions, which are observed in Figure 2b.

Since SWCNTs are bent into nanorings by the water/DCB interface,[8] they represent where the interface is during PE crystallization. Figure 1c shows that, on average, the SWCNTs pass through the center of the PE lamellae; i.e., the lamella width within the DCB droplet is similar to that out of the droplet (d_{in} and d_{out} in Figure 1c, inset), suggesting that during the crystal growth the radial growth rates of PE lamellae toward the DCB and water phase are similar. This is intriguing as the interfacial energies of DCB/PE and water/PE are significantly different [4.3 and 43.3 mN/m, respectively (see SI)]. To further confirm this observation, NHSK nanorings with various PE lamellar sizes were obtained using different PE/SWCNTs weight ratios, varying from 10:1 to 50:1. Figure 3 shows that, as
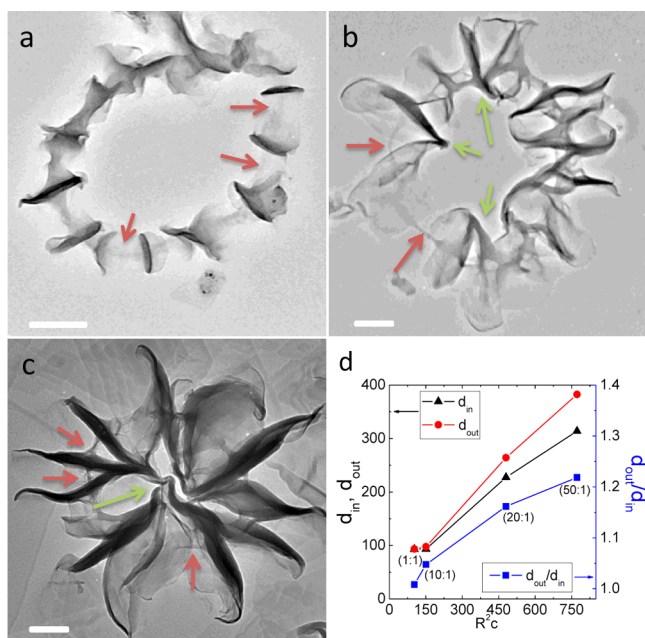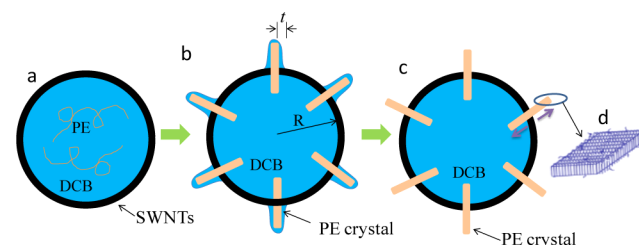

Figure 3. NHSK rings made with different PE/SWCNT weight ratios: (a) 10:1; (b) 20:1; and (c) 50:1. Scale bar is 200 nm. (d) Plot of the outer and inner kebab width and their ratio versus reduced PE concentration. The reduced PE concentration is controlled by varying the feeding ratio of PE and SWCNT from 1:1, 10:1, 20:1 to 50:1.

the PE/SWCNT weight ratio increases, the PE lamellar crystal size increases from ca. 200 nm for 10:1 to ca. 700 nm for 50:1. Even when one side of the PE lamellae reaches the center of the ring, the lamellae remain relatively symmetric (red arrow points to the SWCNTs) about the tube. Figure 3d plots d_{out}, d_{in}, as well as their ratio versus the reduced PE concentration, $Vc/2\pi R \sim R^2c$, where R is the radius of the ring (DCB droplet), V the volume of the DCB droplet, and c the PE concentration. When the PE/SWCNT ratio = 1:1 and 10:1, d_{out} and d_{in} are the same within the experimental error. When the ratio increases to 20:1 and 50:1, crystal growth fronts in the droplet start to interfere inside the droplet (green arrows in Figures 3b and c), and d_{out} becomes slightly greater than d_{in}, reaching a d_{out}/d_{in} of ~1.2 .

These results confirm that PE single crystals have similar growth rates in water and DCB phases during emulsion solution crystallization.

Similar growth rates of PE lamellae in two distinct liquid phases mean that, at the growth fronts within and outside of the DCB droplet, PE concentration and diffusion rates are similar. To explain this intriguing phenomenon, we postulate that an undulated DCB droplets is formed during the single crystal growth process. As shown in Scheme 2, during the

Scheme 2. NHSK Ring Formation Mechanism[a]

[a](a) SWCNTs wrapping around the DCB droplet and PE dissolves in the DCB droplet; (b) PE crystals grow at the undulated water/DCB interface; (c) NHSK rings with the outer PE crystals directly contacting the water phase; (d) PE chains align parallel to the CNT axis.

emulsification process at high temperature, SWCNTs wrap around the water/DCB interface, and PE dissolves in the DCB phase. After being quenched to room temperature, PE starts to nucleate onto the surface of the SWCNTs. At this stage, the water/DCB interface also starts to become undulated to accommodate PE crystal "protrusion" into the water phase from SWCNTs. This rough interface also provides a physical path for PE chains to diffuse to the crystal growth front, similar to polymer thin film crystallization.[13] As the PE crystals further grow, the water/DCB interface continues to deform until the completion of the crystallization (Scheme 2b). To confirm this postulation, we first estimated the amount of DCB needed to protrude into the original water phase and cover the undulated interface (noted as V_{inter}). We assume the original DCB droplet radius R does not change during the entire crystallization process (because once the crystallization takes place the PE crystals physically lock the SWCNT ring, which pins the L/L interface); the total fold surface area of the PE crystal is S; the thickness of the DCB layer to cover the side of the PE crystals is t; and the number of PE crystals in one ring is N (as shown in Scheme 2b). Considering symmetrical distribution of kebab crystals around the tube, the percentage of the DCB that is required to provide the polymer diffusion path can therefore be estimated using eq 1

$$\frac{V_{inter}}{V_{droplet}} \approx \frac{StN}{\frac{4}{3}\pi R^3} \qquad (1)$$

For a typical NHSK ring, $S = \sim 40\,000$ nm^2, $N \sim 15-50$, and $R \sim 0.5-1$ μm, assuming a DCB layer of ~20 nm leads to $V_{inter}/V_{droplet} < 1\%$. Thus, the DCB droplet just needs to slightly deform to provide a diffusion path for PE chains.

Second, we calculate the free energy difference among the three states shown in Scheme 2. Scheme 2a shows the system before PE crystallization. Scheme 2b and 2c represent the states after PE crystallization. The PE lamellae in the water phase are covered with a thin layer of DCB in Scheme 2b, whereas they

are in direct contact with water in Scheme 2c. Since PE concentration is very low and the lateral surface free energy can be neglected, the free energy changes can be calculated as follows.

From a to b

$$\Delta G_{a \to b} = \Delta G_{interface} - \Delta G_{crystallization}$$

$$= (SN\gamma_{PE/DCB} + 0.5SN\gamma_{DCB/H_2O}) - \Delta Hn \qquad (2)$$

From b to c

$$\Delta G_{b \to c} = 0.5SN(\gamma_{PE/H_2O} - \gamma_{PE/DCB} - \gamma_{DCB/H_2O}) \qquad (3)$$

ΔH is the heat of fusion of PE, which is 3.430 kJ/mol at 300 K,[14] and n is the moles of PE repeating units in one NHSK ring. $\gamma_{PE/DCB}$ = 4.3 mN/m (see SI), γ_{DCB/H_2O} = 40 mN/m, γ_{PE/H_2O} = 43.3 mN/m (see SI), therefore $\Delta G_{a \to b}$ = −1.17 × $10^9 k_B T$ and $\Delta G_{b \to c}$ = −2.43 × $10^5 k_B T$.

The above calculation shows that Scheme 2c is the global minimum energy state, although the free energy difference between Scheme 2b and 2c is small $[(\gamma_{PE/H_2O} - \gamma_{PE/DCB} - \gamma_{DCB/H_2O}) \sim 0]$. Nevertheless, the undulated L/L interface in Scheme 2b facilitates PE free chains to diffuse to the growth front of the lamellae outside the SWCNT ring and leads to a relatively symmetrical PE lamellae around SWCNTs. The energy gain upon crystallization is significantly greater compared with the surface free energy penalty upon creating the undulated interface, and Scheme 2b therefore is the intermediate state for interface crystallization.

In summary, NHSK nanorings have been formed using a PE/SWCNTs/DCB/water system, where SWCNTs are used as the Pickering emulsion agents. SWCNTs are bent to nanorings by the curved DCB/water interface. These SWCNTs nucleate PE crystallization upon cooling, leading to NHSK nanorings. PE lamellae are perpendicular to the SWCNT axis, indicating that the crystal growth is orthogonal to the DCB/water interface. More interestingly, the growth rates of PE lamellae within and out of the DCB droplets are similar. We attribute this observation to the undulated DCB/water interface induced by PE crystal growth.

■ ASSOCIATED CONTENT

Ⓢ Supporting Information
Detailed experimental procedures and tomography recon-structed movie. This material is available free of charge via the Internet at http://pubs.acs.org.

■ AUTHOR INFORMATION

Corresponding Author
*E-mail: chrisli@drexel.edu.

Notes
The authors declare no competing financial interest.

■ ACKNOWLEDGMENTS

■ REFERENCES

(1) (a) Keller, A.; Cheng, S. Z. D. *Polymer* **1998**, *39*, 4461−4487. (b) Lotz, B.; Cheng, S. Z. D. *Polymer* **2005**, *46*, 577−610. (c) Hong, S.; Zhang, X.; Zhang, R.; Wang, L.; Zhao, J.; Han, C. C. *Macromolecules* **2008**, *41*, 2311−2314. (d) Mitra, M. K.; Muthukumar, M. *J. Chem. Phys.* **2010**, *132*, 184908. (e) Shi, W.; Cheng, H.; Chen, F.; Liang, Y.; Xie, X.; Han, C. C. *Macromol. Rapid Commun.* **2011**, *32*, 1886−1890. (f) Shi, W.; Yang, J.; Zhang, Y.; Luo, J.; Liang, Y.; Han, C. C. *Macromolecules* **2012**, *45*, 941−950.

(2) (a) Schaaf, P.; Lotz, B.; Wittmann, J. C. *Polymer* **1987**, *28*, 193−200. (b) Hu, W.; Frenkel, D.; Mathot, V. B. F. *J. Chem. Phys.* **2003**, *118*, 10343−10348. (c) Hu, W.; Frenkel, D. *Macromolecules* **2004**, *37*, 4336−4338. (d) Morimoto, N.; Obeid, R.; Yamane, S.; Winnik, F. M.; Akiyoshi, K. *Soft Matter* **2009**, *5*, 1597−1600. (e) Obeid, R.; Tanaka, F.; Winnik, F. o. M. *Macromolecules* **2009**, *42*, 5818−5828. (f) Zha, L.; Hu, W. *Polymer* **2009**, *50*, 3828−3834. (g) Diehl, C.; Cernoch, P.; Zenke, I.; Runge, H.; Pitschke, R.; Hartmann, J.; Tiersch, B.; Schlaad, H. *Soft Matter* **2010**, *6*, 3784−3788. (h) Schlaad, H.; Diehl, C.; Gress, A.; Meyer, M.; Demirel, A. L.; Nur, Y.; Bertin, A. *Macromol. Rapid Commun.* **2010**, *31*, 511−525.

(3) Pickering, S. U. *J. Chem. Soc. Trans.* **1907**, *91*, 2001−2021.

(4) Boker, A.; He, J.; Emrick, T.; Russell, T. P. *Soft Matter* **2007**, *3*, 1231−1248.

(5) (a) Velev, O. D.; Furusawa, K.; Nagayama, K. *Langmuir* **1996**, *12*, 2374−2384. (b) Dinsmore, A. D.; Hsu, M. F.; Nikolaides, M. G.; Marquez, M.; Bausch, A. R.; Weitz, D. A. *Science* **2002**, *298*, 1006−1009. (c) Duan, H.; Wang, D.; Kurth, D. G.; Möhwald, H. *Angew. Chem., Int. Ed.* **2004**, *43*, 5639−5642. (d) Lin, Y.; Skaff, H.; Emrick, T.; Dinsmore, A. D.; Russell, T. P. *Science* **2003**, *299*, 226−229. (e) Reincke, F.; Hickey, S. G.; Kegel, W. K.; Vanmaekelbergh, D. *Angew. Chem., Int. Ed.* **2004**, *43*, 458−462.

(6) He, J.; Zhang, Q.; Gupta, S.; Emrick, T.; Russell, T.; Thiyagarajan, P. *Small* **2007**, *3*, 1214−1217.

(7) (a) Wang, R. K.; Park, H.-O.; Chen, W.-C.; Silvera-Batista, C.; Reeves, R. D.; Butler, J. E.; Ziegler, K. J. *J. Am. Chem. Soc.* **2008**, *130*, 14721−14728. (b) Wang, R. K.; Reeves, R. D.; Ziegler, K. J. *J. Am. Chem. Soc.* **2007**, *129*, 15124−15125. (c) Wang, H.; Hobbie, E. K. *Langmuir* **2003**, *19*, 3091−3093. (d) Matsui, J.; Yamamoto, K.; Miyashita, T. *Carbon* **2009**, *47*, 1444−1450.

(8) Wang, W.; Laird, E. D.; Gogotsi, Y.; Li, C. Y. *Carbon* **2012**, *50*, 1769−1775.

(9) (a) Li, L.; Li, B.; Hood, M. A.; Li, C. Y. *Polymer* **2009**, *50*, 953−965. (b) Laird, E. D.; Li, C. Y. *Macromolecules* **2013**, *46*, 2877−2891. (c) Li, C. Y. *J. Polym. Sci., Part A: Polym. Phys.* **2009**, *47*, 2436−2440. (d) Grady, B. P. *J. Polym. Sci., Part B: Polym. Phys.* **2012**, *50*, 591−623. (e) Ning, N.; Fu, S.; Zhang, W.; Chen, F.; Wang, K.; Deng, H.; Zhang, Q.; Fu, Q. *Prog. Polym. Sci.* **2012**, *37*, 1425−1455.

(10) (a) Li, L. Y.; Li, C. Y.; Ni, C. Y.; Rong, L. X.; Hsiao, B. *Polymer* **2007**, *48*, 3452−3460. (b) Li, L. Y.; Li, B.; Yang, G. L.; Li, C. Y. *Langmuir* **2007**, *23*, 8522−8525. (c) Li, L.; Yang, Y.; Yang, G.; Chen, X.; Hsiao, B. S.; Chu, B.; Spanier, J. E.; Li, C. Y. *Nano Lett.* **2006**, *6*, 1007−1012. (d) Li, L.; Li, C. Y.; Ni, C. Y. *J. Am. Chem. Soc.* **2006**, *128*, 1692−1699. (e) Kodjie, S. L.; Li, L. Y.; Li, B.; Cai, W. W.; Li, C. Y.; Keating, M. *J. Macromol. Sci., Part B: Phys.* **2006**, *45*, 231−245. (f) Li, C. Y.; Li, L.; Cai, W.; Kodjie, S. L.; Tenneti, K. K. *Adv. Mater.* **2005**, *17*, 1198−1202. (g) Laird, E. D.; Bose, R. K.; Wang, W.; Lau, K. K. S.; Li, C. Y. *Macromol. Rapid Commun.* **2013**, *34*, 251−256. (h) Wang, W.; Laird, E. D.; Li, B.; Li, L.; Li, C. Y. *Sci. China Chem.* **2012**, *55*, 802−807. (i) Laird, E. D.; Wang, W.; Cheng, S.; Li, B.; Presser, V.; Dyatkin, B.; Gogotsi, Y.; Li, C. Y. *ACS Nano* **2012**, *6*, 1204−1213. (j) Li, L.; Wang, W.; Laird, E. D.; Li, C. Y.; Defaux, M.; Ivanov, D. A. *Polymer* **2011**, *52*, 3633−3638. (k) Li, B.; Li, L. Y.; Wang, B. B.; Li, C. Y. *Nature Nanotechnol.* **2009**, *4*, 358−362.

(11) Jinnai, H.; Spontak, R. J.; Nishi, T. *Macromolecules* **2010**, *43*, 1675−1688.

(12) (a) Chen, X.; Wang, W.; Cheng, S.; Dong, B.; Li, C. Y. *ACS Nano* **2013**, *7*, 8251−8257. (b) Chen, X.; Dong, B.; Wang, B. B.; Shah, R.; Li, C. Y. *Macromolecules* **2010**, *43*, 9918−9927. (c) Wang, B. B.; Li, B.; Xiong, J.; Li, C. Y. *Macromolecules* **2008**, *41*, 9516−9521.

(13) Li, C. Y.; Ge, J. J.; Bai, F.; Calhoun, B. H.; Harris, F. W.; Cheng, S. Z. D.; Chien, L. C.; Lotz, B.; Keith, H. D. *Macromolecules* **2001**, *34*, 3634−3641.

(14) Gaur, U.; Wunderlich, B. *J. Phys. Chem. Ref. Data* **1981**, *10*, 119−152.